Journal of
Polymer Materials

Tech Science Press

http://doi.org/10.32604/jpm.2026.089087

ARTICLE

HAPAM-Based Slickwater Fracturing Fluid Reinforced by Active Silicon Quantum Dots: Polymer-QD Interaction Mechanism, Rheological Regulation and Imbibition Oil Displacement Performance

Yuan Xu[1], Rui Jiang[1], Shuowen Deng[1], Kun Ding[2], Zheng Yao[3], Yifeng Liao[4], Youquan Liu[1], Qi Xu[4] and Daijun Du[4,*]

[1]Research Institute of Natural Gas Technology, PetroChina Southwest Oil & Gas Field Company, Chengdu, China
[2]Engineering Technology Department, PetroChina Xinjiang Oilfield Company, Karamay, China
[3]North Part of Central Sichuan Gas Production Management, PetroChina Southwest Oil & Gas Field Company, Suining, China
[4]State Key Laboratory of Oil and Gas Reservoir Geology and Exploitation, Southwest Petroleum University, Chengdu, China
*Corresponding Author: Daijun Du. Email: axiaodu1991@163.com

Received: 21 July 2026; Accepted: 22 September 2026; Online first: 14 October 2026

ABSTRACT: Hydrophobically associating polyacrylamide (HAPAM) serves as the core thickening polymer of slickwater fracturing fluid for tight oil stimulation, yet conventional HAPAM slickwater suffers from weak network structure, insufficient viscoelasticity and limited spontaneous imbibition oil-displacement capacity. Fracturing-displacement integration technology relies on polymer fluid's rheological and interfacial performance to boost tight oil recovery, while polymer-nanomaterial synergistic modification is a key research direction for polymer fracturing fluid optimization. In this work, amphiphilic active silicon quantum dots (SiQDs) were compounded with HAPAM polymer slickwater to construct a polymer-quantum dot composite multifunctional fracturing fluid (SQDMFF), with a focus on revealing the supramolecular interaction mechanism between HAPAM molecular chains and surface-functionalized SiQDs. Surface-modified SiQDs adsorb onto HAPAM backbones and self-assemble into aqueous micelles, crosslinking with hydrophobic segments of HAPAM via non-covalent supramolecular forces, which densifies the polymer three-dimensional network and enhances the polymer fluid's viscosity, viscoelasticity and proppant transport performance. The extra osmotic pressure induced by SiQDs further strengthens the rock surface oil-stripping capacity of the HAPAM polymer system. After gel breaking of the composite polymer fluid, the oil-water interfacial tension is reduced to 10^{-2} mN/m magnitude, and the rock-oil-fluid three-phase contact angle declines from 102.7° to 44.8°, realizing effective oil-wet to water-wet wettability alteration. Static core spontaneous imbibition experiments prove the composite polymer fracturing fluid achieves an ultimate imbibition oil recovery of 35.2%. This study provides theoretical guidance for the performance modification of polymer fracturing fluids and exhibits promising application potential for fracturing-displacement combined development of tight oil reservoirs.

KEYWORDS: Hydrophobically associating polyacrylamide (HAPAM); polymer fracturing fluid; silicon quantum dots; polymer-nanoparticle interaction; slickwater; imbibition oil displacement; wettability alteration; tight oil reservoir

1 Introduction

Tight reservoirs are generally characterized by poor physical properties, complex pore-throat structures, and extremely low matrix permeability [1–3]. Under overburden pressure, these formations typically exhibit porosity below 10%, pore-throat diameter of less than 1 μm, and a permeability lower than 0.1 mD [4,5]. As a result, field development often faces significant challenges, including rapid production decline in

Copyright © 2026 The Authors. Published by Tech Science Press. This work is licensed under a Creative Commons Attribution 4.0 International License, which permits unrestricted use, distribution, and reproduction in any medium, provided the original work is properly cited.

individual wells, inefficient reservoir utilization, and low primary recovery factors [6,7]. Consequently, to achieve economically viable production from tight oil resources, additional reservoir stimulation is typically required after drilling and completion. Among the various stimulation techniques, hydraulic fracturing has emerged as one of the most widely adopted methods for enhancing productivity in tight reservoirs [8]. This technique involves injecting a viscous fracturing fluid—typically blended with chemical additives—into the target formation via high-pressure surface pumps. The injected fluid artificially creates and propagates fractures, thereby effectively improving crude oil flow through the matrix pore network [9,10]. The resulting high-conductivity propped fractures serve as efficient drainage channels, substantially facilitating fluid transport from the low-permeability matrix toward production wells. Thus, successful fracturing treatments are generally expected to lead to increased well productivity [11]. Slickwater fracturing fluid dominated by hydrophobically associating polyacrylamide (HAPAM) polymer has become the primary stimulation fluid for tight oil volume fracturing. As a typical associative water-soluble polymer, HAPAM forms physical crosslinking networks through intermolecular hydrophobic association, endowing base slickwater with basic viscosity and sand-carrying capacity. Nevertheless, the pure HAPAM polymer network presents low crosslink density under reservoir high-temperature conditions; the loose polymer skeleton is prone to chain disentanglement, leading to rapid viscosity attenuation, weak elastic modulus, and poor long-term proppant suspension performance. Meanwhile, single HAPAM polymer solution lacks efficient interfacial regulation capability, failing to substantially lower oil-water interfacial tension or reverse rock wettability, which fundamentally causes the rapid post-fracturing production decline of tight oil wells. Modifying HAPAM polymer fracturing fluids via nanoscale functional fillers has become a mainstream strategy to overcome the inherent limitations of pure polymer systems in polymer materials research. However, field practice has revealed that not all wells with successfully created conductive fractures exhibit a notable increase in production following treatment. In some cases, the incremental oil gain remains marginal, and in certain instances, post-fracturing production may even decline. This discrepancy underscores the complexity of fracture-matrix interaction and suggests that fracture creation alone does not guarantee effective reservoir drainage, highlighting the need for a more nuanced understanding of the underlying mechanisms governing stimulation performance.

Currently, slickwater-based volume fracturing remains the predominant stimulation strategy for the development of such reservoirs. This approach substantially enlarges the drainage area through the creation of complex fracture networks in the subsurface [12–14]. Nevertheless, field applications frequently encounter the phenomenon of "high initial productivity followed by a rapid decline". The underlying cause is primarily attributed to the inadequate regulation of interfacial energy among the oil, water, and rock phases during the fracturing process. This deficiency impedes the long-term stability of the established flow conduits, thereby compromising the sustained effectiveness of the stimulation treatment [15–17].

To mitigate the aforementioned issue of production decline, the integrated "fracturing-displacement" concept has recently been proposed as a promising technical strategy [18]. This approach incorporates surfactant-based imbibition agents into the slickwater system. On one hand, these agents reduce the oil-water interfacial tension and modify reservoir wettability, thereby activating capillary-driven imbibition. Previous studies have demonstrated that such modifications can improve imbibition efficiency by approximately 20%. On the other hand, the adsorption of surfactant molecules onto proppant and rock surfaces effectively lowers the interfacial energy at these solid-fluid interfaces, which helps inhibit fracture closure and decelerates the decline in fracture conductivity. Collectively, this technology synergistically combines the capacity of slickwater to generate complex fracture networks with a sustained displacement function, offering a novel pathway for achieving prolonged post-fracturing production in tight oil reservoirs [19–22].

However, conventional surfactants exhibit inherent limitations in regulating interfacial energy. As reported in Nature, the Nikolov-Wasan model indicates that systems such as nanofluids, globular micellar fluids, and globular protein fluids generate additional osmotic pressure during the displacement process. The resultant disjoining pressure enables these systems to strip oil films from solid surfaces with substantially higher efficiency than conventional small-molecule active fluids [23]. Furthermore, the model theoretically predicts that, under reservoir conditions, the optimal oil-displacement performance of nanofluids relies on the preservation of two critical attributes: ultradispersibility and ultrasmall particle size. Among the available nanomaterials, quantum dots are classified as "zero-dimensional nanomaterials" as their three-dimensional sizes (typically below 10 nm) fall below the exciton Bohr radius of the base material, which also confers unique fluorescent properties. This dimensional characteristic places quantum dots at the current technological frontier in particle size miniaturization [24–26]. On this basis, the present study introduces active silicon quantum dots into field-applied slickwater to formulate a multifunctional fracturing–displacement system. The effects of active silicon quantum dots on the rheological and interfacial properties of the slickwater are systematically investigated, and the imbibition efficiency of the resulting system is evaluated. This work is expected to provide both theoretical insights and technical references for fracture stimulation practices in tight oil reservoirs.

2 Materials and Methods

2.1 Active Silicon Quantum Dots and Slick Water

Active silicon quantum dots (active SiQDs) were synthesized following the procedure reported in the literature, with the synthetic route illustrated in Fig. 1. In this scheme, GA denotes glutaraldehyde, SPS represents sodium p-aminobenzenesulfonate, and OGE refers to octyl glycidyl ether. The base SiQDs were prepared from sodium citrate and 3-aminopropyltriethoxysilane, which were subsequently functionalized to yield the active SiQDs.

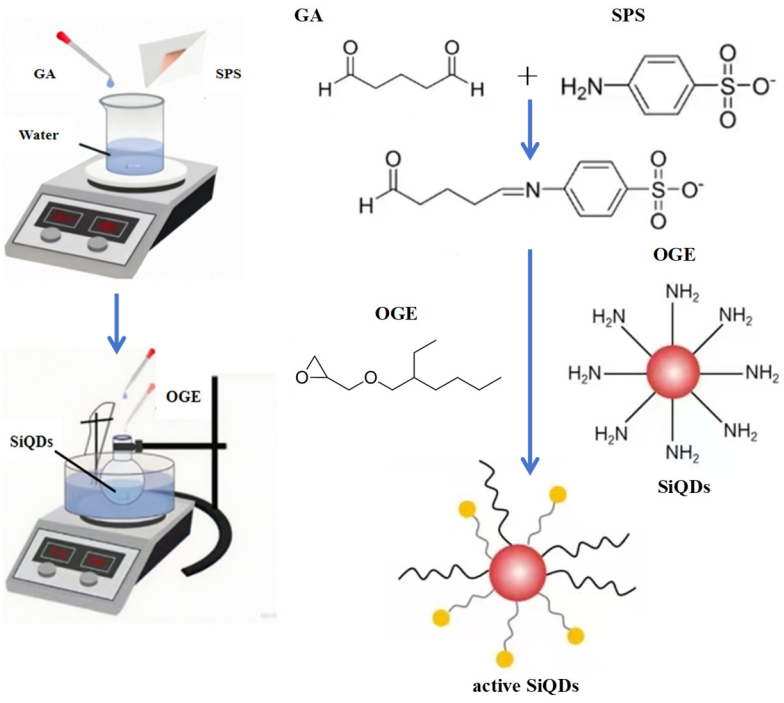


Figure 1: Synthesis route of active silicon quantum dots.

The micromorphology, particle size distribution, FT-IR spectra of the as-prepared active SiQDs are presented in Fig. 2. The particles are predominantly spherical or nearly spherical in shape, with a minor fraction exhibiting elliptical or irregular morphologies. The sample shows good dispersibility, and no noticeable agglomeration is observed. The average particle size is approximately 5 nm, with a relatively narrow size distribution. The band at 3300 cm^{-1} is attributed to O-H or N-H stretching vibrations. The peaks at 1550 and 1459 cm^{-1} correspond to C=C skeletal vibrations of the aromatic ring. The band at 1380 cm^{-1} is assigned to the asymmetric S=O stretching vibration, while the peak at 1200 cm^{-1} arises from the symmetric S=O stretching vibration. The band at 1033 cm^{-1} is due to the Si-O-Si stretching vibration, and the peak at 890 cm^{-1} is attributed to the out-of-plane C-H bending vibration of the aromatic ring. The presence of characteristic benzenesulfonic acid peaks in the infrared spectrum indicates that benzenesulfonic acid groups have been successfully grafted onto the surface of the silicon quantum dot support.

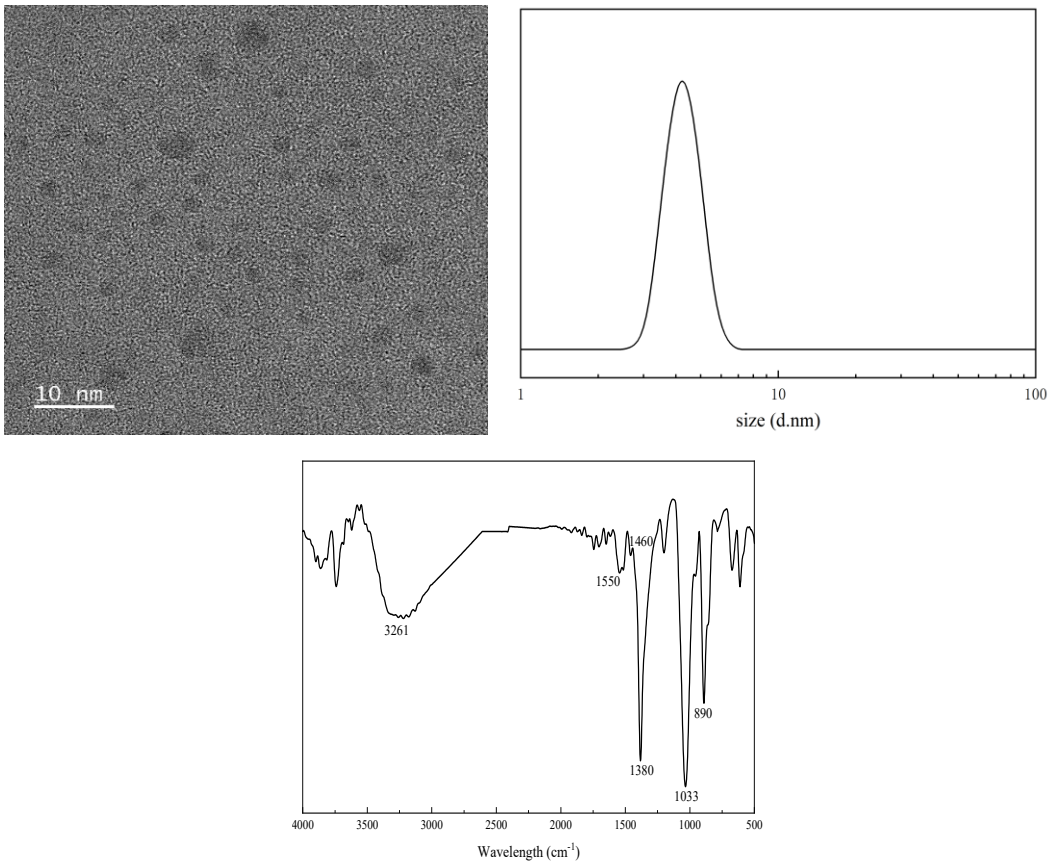


Figure 2: Micromorphology, particle size distribution and FT-IR spectra of the SiQDs.

The slickwater fracturing fluid was provided by the Research Institute of Natural Gas Technology, PetroChina Southwest Oil & Gas Field Company. Its formulation comprises 0.2% hydrophobically associating polyacrylamide (HAPAM) as the thickener, 0.2% flowback aid, 0.1% gel breaker, and fresh water. The molecular structure of HAPAM is shown in Fig. 3. Core samples used in this study were obtained from the Shunqing Oilfield in the Sichuan Basin, China. The matrix porosity and gas permeability were measured as 4.8% and 0.034 mD, respectively, following the standard procedure specified in SY/T 5336-2006 [27].

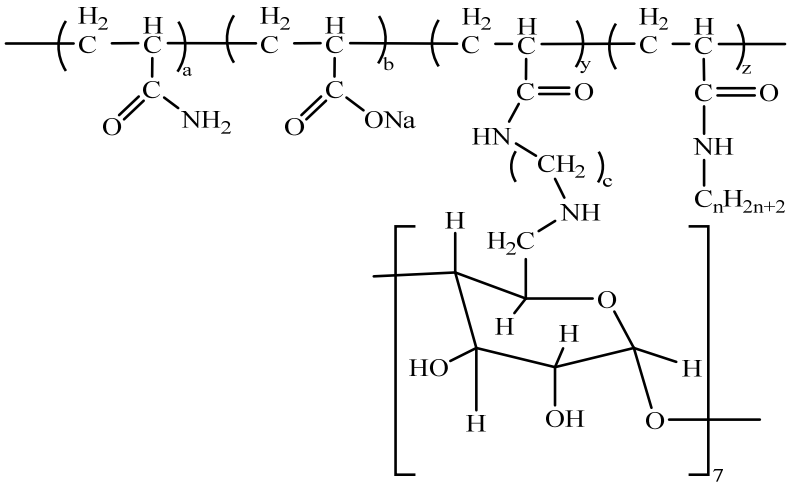


Figure 3: Molecular structure of HAPAM (viscosity-average molecular weight is 625×10^4 g/mol).

2.2 Preparation of Polymer-Quantum Dot Composite Multifunctional Fracturing Fluid (SQDMFF)

The base slickwater fracturing fluid was prepared as follows: 1 g of HAPAM was dissolved in 500 mL of fresh water under continuous stirring. After complete dissolution, 1 g of flowback aid and 0.5 g of gel breaker were sequentially added, and the mixture was stirred mechanically for 10 min to prevent agglomeration of the additives. The resulting solution was designated as the base slickwater fracturing fluid and reserved for subsequent use. To prepare SQDMFF, 10 mL of a 10% (w/w) active SiQDs dispersion was introduced into the base fluid under stirring, and the mixture was agitated for an additional 30 min to ensure uniform dispersion and system stability. At this SiQDs concentration, its incorporation did not adversely affect the viscosity or proppant-carrying performance of the base slickwater.

2.3 Microstructural Characterization

The microscopic morphologies of SQDMFF and the field-applied slickwater were characterized using an environmental scanning electron microscope (ESEM). The sample preparation procedure was as follows: approximately 1–10 μL of the fluid sample was transferred onto a substrate using a micropipette. The specimen was then rapidly frozen with liquid nitrogen and subsequently freeze-dried. To improve image quality, a thin gold layer was sputter-coated onto the dried sample surface. Under an appropriate magnification, the contrast and brightness were carefully adjusted to optimize imaging conditions. High-resolution micrographs were then captured and stored for further analysis.

2.4 Slickwater Performance

Rheological Properties. The viscoelastic properties of SQDMFF and the field-applied slickwater were characterized using a high-temperature high-pressure rheometer at the reservoir temperature (70°C) and atmospheric pressure, with an oscillatory frequency sweep conducted over the range of 0.1 Hz to 10 Hz (strain amplitude, 1%, determined from strain sweep tests within the linear viscoelastic region, LVER, which was confirmed to be ≤5%). In addition, the apparent viscosity of both fluid systems was measured at a shear rate of 170 s^{-1} using the same instrument. All measurements were performed in triplicate; mean values are reported.

Proppant-Carrying Capacity. The proppant transport performance of SQDMFF was evaluated using a large-scale visualized fracture simulation system equipped with parallel plates. Experiments were

conducted at room temperature and a constant pumping rate of 4 m^3/min, with proppant concentrations varying across four levels: 20%, 30%, 40%, and 50%. For each test, the SQDMFF was freshly prepared, a designated amount of proppant was weighed, and the valve configuration was adjusted to achieve the required flow path status. The initial fracture width was set to 8 mm. After pumping was completed and the proppant bank morphology within the fracture had stabilized, images of the experimental results were captured with careful attention to data integrity. Subsequently, the proppant bank contours were extracted from the images, and the settling velocity of the quartz sand was calculated based on the acquired data. As a control, the proppant-carrying experiment with a proppant concentration of 20% was conducted using the base slickwater. All measurements were performed in triplicate; mean values are reported.

SQDMFF—Crude Oil–Rock Interactions. The oil-water interfacial tension (IFT) reduction capability of SQDMFF, both before and after gel breaking, was evaluated using an interfacial tensiometer based on the spinning drop method. To obtain the gel-breaking fluid, the prepared SQDMFF was placed in a constant-temperature oven at 70°C for 3 h, which allowed the thermal decomposition of the gel breaker and the subsequent cleavage of polymer chains. Field-produced crude oil was first dehydrated using an automatic dehydrator, and the resulting dehydrated oil sample was stored under vacuum prior to use. In the measurement procedure, the sample tube was filled with the test fluid using a microsyringe to ensure complete removal of air, after which a small oil droplet was injected into the tube. IFT measurements were conducted at 70°C and a rotational speed of 6000 rpm. All measurements were performed in triplicate; mean values are reported. The wettability alteration ability of SQDMFF after gel breaking was assessed using a shape analyzer. Oil-wet rock slides were prepared by immersing clean rock slice in crude oil for 24 h, after which they were removed, gently wiped with lens paper to remove excess oil, rinsed with distilled water, and dried. The prepared oil-wet slides were then immersed in the gel-breaking fluid and placed in an oven at 70°C. At predetermined time intervals, the slides were retrieved, and the three-phase contact angles among the rock surface, crude oil, and test fluid were measured.

Imbibition Recovery Factor. The pore-throat-scale oil mobilization behavior of SQDMFF during imbibition after gel breaking was characterized using high-temperature high-pressure online nuclear magnetic resonance (NMR) displacement, with deuterium oxide (D_2O) used as the solvent for sample preparation. The experimental procedure was as follows: The core sample was first dried at 90°C until a constant weight was achieved, and the dry weight (m_1) was recorded. The permeability and porosity of the core were then measured. Subsequently, the core was saturated with dehydrated crude oil under vacuum using a molecular pump. After saturation, the core was removed, excess oil on the surface was wiped off, and the weight of the oil-saturated core (m_2) was recorded. The initial oil content in the core was determined from the weight difference before and after oil saturation ($m_2 - m_1$) and density.

The oil-saturated core was then placed in an imbibition cell containing the D_2O-based test system, and the cell was maintained at 70°C in an oven. T_2 spectra of the core were acquired at predetermined time intervals until no further oil production was observed. The imbibition recovery factor was determined based on the reduction in the integrated T_2 spectral area, which was pre-calibrated against the initial oil volume obtained from gravimetric measurements.

3 Results and Discussion

3.1 Microstructure of Slickwater

The microstructures of the field-applied slickwater and SQDMFF are compared in Fig. 4. The ESEM images indicate a denser and more interconnected morphology in the freeze-dried SQDMFF compared to the base slickwater, which suggests a more robust polymer network in the original fluid. First, electrostatic

adsorption between SiQDs and HAPAM backbones: Active SiQDs carry abundant positively charged amino groups on the surface, while the amide and carboxyl group segments of HAPAM polymer exhibit weak negative charges. Electrostatic attraction drives SiQDs to uniformly adsorb onto HAPAM molecular chains, restricting intramolecular curling of polymer chains and inhibiting the collapse of the original loose HAPAM network. Second, hydrophobic association crosslinking between SiQD micelles and HAPAM hydrophobic segments: amphiphilic SiQDs self-assemble into nano-micelles in aqueous polymer solution. The long alkyl hydrophobic branches on SiQD surfaces form inter-molecular hydrophobic association with the hydrophobic side chains of HAPAM, building extra physical crosslinking points inside the polymer network. The dual effects fill the voids of the original HAPAM polymer skeleton, raise the crosslink density of the whole polymer network, and greatly improve the structural integrity of the HAPAM slickwater system. This polymer-quantum dot reinforcement mechanism is no longer limited to macroscopic morphological inference, and direct microscopic interfacial characterization data can quantitatively confirm the above interaction pathways.

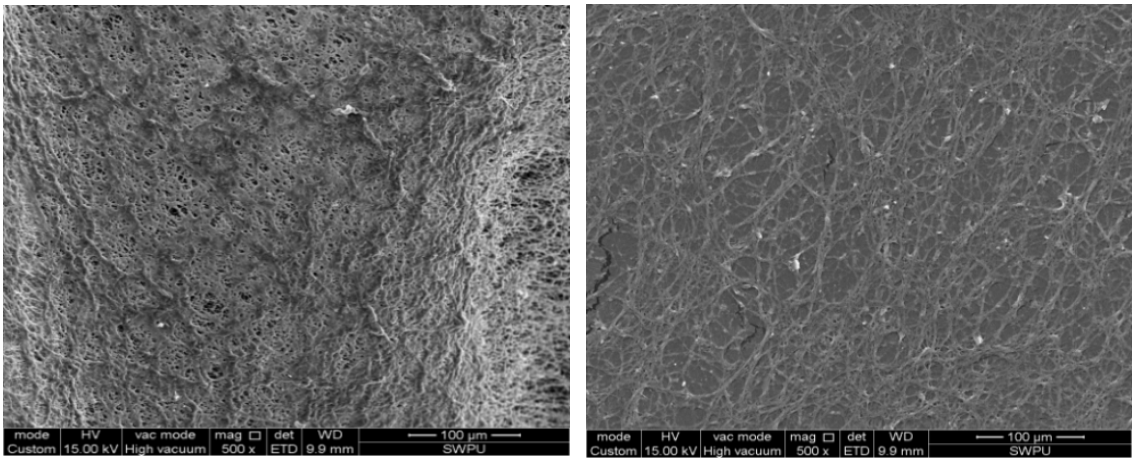


Figure 4: Micro-morphologies of on-site slickwater and SQDMFF.

3.2 Rheological Properties of the Multifunctional Pressure-Driven System

The viscoelastic properties of the field-applied slickwater and SQDMFF are compared in Fig. 5. Upon the addition of active silicon quantum dots, both the storage modulus (G′) and loss modulus (G″) of the system increased across the entire tested frequency range. Moreover, the crossover frequency, at which G′ and G″ intersect, shifted toward a higher value, indicating a pronounced enhancement in the elastic response of SQDMFF. This transition reflects an increase in structural strength and suggests improved proppant-suspending capability, which is favorable for proppant transport during fracturing operations.

Fig. 6 presents the viscosity-temperature profiles of the field-applied slickwater and SQDMFF. For both systems, viscosity decreases progressively with increasing temperature. However, SQDMFF consistently exhibits higher viscosity than the base slickwater across the entire temperature range tested. This enhancement is mainly attributable to the incorporation of active silicon quantum dots, which reinforce the three-dimensional network structure through adsorption onto polymer chains and supramolecular crosslinking interactions. Such structural reinforcement restricts the mobility of polymer molecular chains, thereby resulting in elevated viscosity. These observations are in good agreement with the microstructural and viscoelasticity results discussed above.

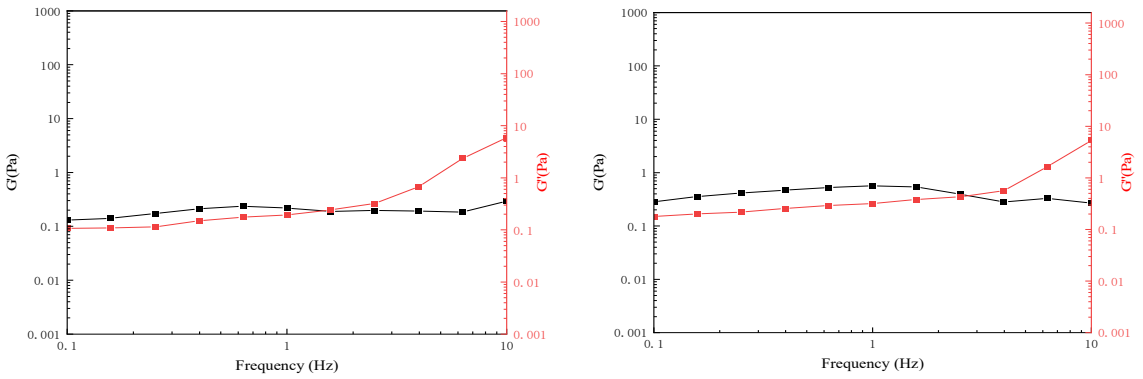


Figure 5: Viscoelasticity of on-site slickwater and SQDMFF before and after the addition of active silicon quantum dots.

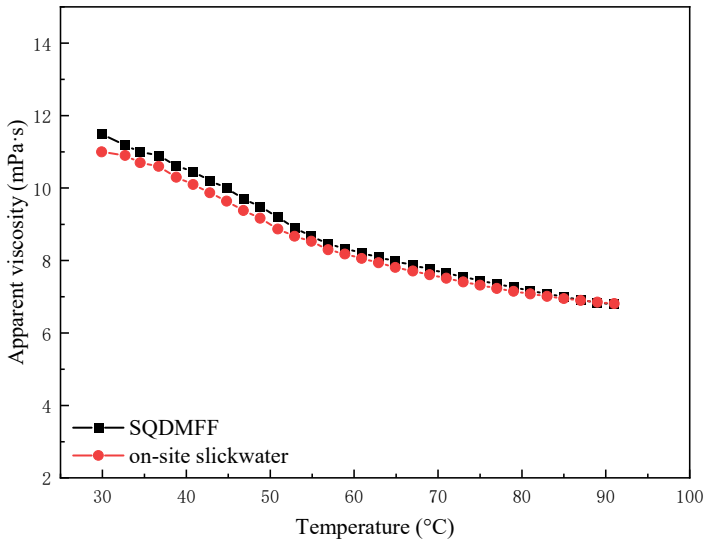


Figure 6: Viscosity-temperature behavior of on-site slickwater and SQDMFF.

3.3 Proppant-Carrying Capacity of the SQDMFF

The proppant settling rates under different sand ratios and the corresponding sandbank heights at various positions are summarized in Tables 1 and 2, respectively. As the sand ratio increases—indicating a higher proppant concentration within the fracture—inter-particle interactions among the proppant grains are intensified. As a result, the quartz sand settling rate decreases from 3.1 cm/min to 0.5 cm/min, accompanied by an increase in sandbank height and a reduction in its horizontal propagation distance (Fig. 7). Also, results showed that the base slickwater exhibited a settling rate of 3.3 cm/min at 20% sand ratio, which was significantly higher than that of the SQDMFF system (3.1 cm/min), confirming the enhanced proppant-carrying capacity of SQDMFF system, which was ascribed to the enhancement of viscosity and viscoelasticity of SQDMFF. To mitigate the risk of sand plugging during field operations, the sand ratio should be designed following the principle of "low initial concentration followed by gradual increase". This strategy is justified by the fact that while a higher sand ratio promotes effective proppant placement near the wellbore, an excessively high concentration can readily lead to bridging and plugging within the fracture system.

Table 1: Sandbank heights at various positions for SQDMFF.

Proppant Concentration	Position 1	Position 2	Position 3	Position 4
20	24.6	24.8	25.0	25.1
30	34.5	34.7	35.7	36.5
40	39.1	39.3	39.5	41.3
50	46.3	46.5	46.7.	47.6

Table 2: Proppant settling rates at different sand ratios.

System	Proppant Concentration (%)	Average Settling Rate (cm/min)
Base slickwater	20	3.3
SQDMFF	20	3.1
	30	2.1
	40	1.4
	50	0.5

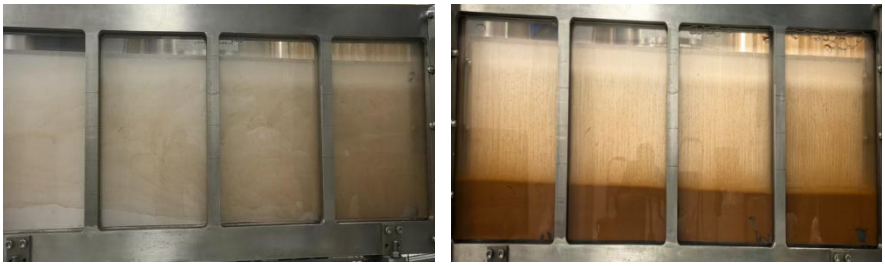


Figure 7: Physical photographs of the proppant-carrying experiment (Positions 1–4 from right to left along the middle line of the visual window).

3.4 Interactions among the SQDMFF, Crude Oil, and Rock

Table 3 presents the interfacial tension measurements between various systems and crude oil. The on-site slickwater exhibits an interfacial tension with crude oils from different wells on the order of 10^0 mN/m. Following the incorporation of active silicon quantum dots, the interfacial tension is reduced to the order of 10^{-1} mN/m. After gel breaking, the oil-water interfacial tension is further lowered to the order of 10^{-2} mN/m. Such low oil-water interfacial tension promotes oil droplet deformation and enhances oil transport efficiency within porous media.

Table 3: Interfacial tension between different systems (each with a friction reducer concentration of 0.2%) and crude oil.

Crude Oil	#1	#2	#3
System		IFT (mN/m)	
After gel breaking of the on-site slickwater	2.1767	2.4764	3.0587
Before gel breaking of SQDMFF	0.4152	0.3601	0.8744
After gel breaking of SQDMFF	0.03176	0.03054	0.03366

As illustrated in Fig. 8, SQDMFF significantly modifies the wettability of the rock surface. This modification is mainly attributed to the active silicon quantum dots present in the system, which effectively displace the crude oil adsorbed onto the rock surface and subsequently adsorb onto the rock surface with their hydrophilic groups facing outward. As a result, the contact angle of the rock decreases to 44.8°. After the rock surface becomes hydrophilic, re-adsorption of crude oil onto the rock surface during migration in porous media is effectively prevented, thereby facilitating crude oil production [28].

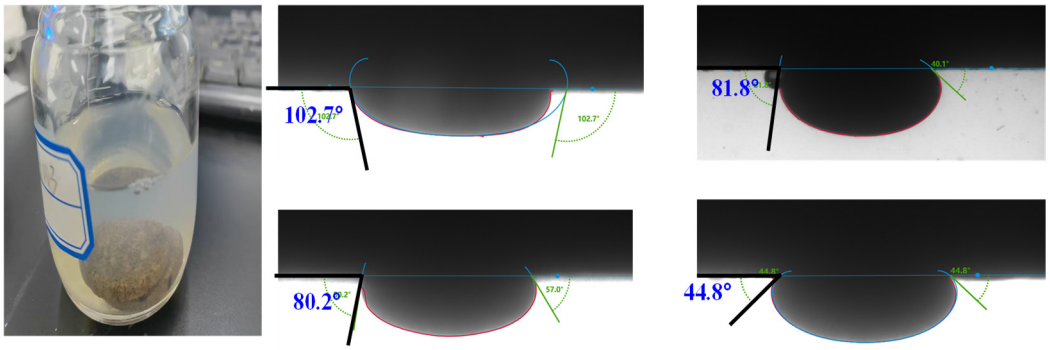


Figure 8: Contact angle variation under different soaking times (crude oil from #3).

According to the classical Nikolov-Wasan model, nanoparticles that are ultrasmall (<10 nm) and well-dispersed in aqueous media can generate a significant structural disjoining pressure at the wedge film region near the three-phase contact line. This mechanism has been further validated in enhanced oil recovery applications, where nanoparticle-induced structural disjoining pressure promotes oil film detachment from solid surfaces. Recent studies have demonstrated that functionalized silicon quantum dots, similar to those employed in our work, exhibit strong interfacial activity and wettability alteration capability, making them promising candidates for EOR applications. The observed reduction in oil-water interfacial tension and contact angle in our study is consistent with these previously reported mechanisms.

3.5 Imbibition Efficiency of the Multifunctional Pressure-Driven System

The core sample parameters are tabulated in Table 4. As presented in Fig. 9, the evolution of T_2 spectra and the corresponding oil recovery during imbibition reveal that within the initial 12 h, oil recovery increases gradually. Upon extending the imbibition time to 9 days, a rapid increase in oil recovery from 10.1% to 25.5% is observed. When the imbibition time reaches 11 days, the oil recovery attains 35.2%. Two-dimensional imaging at various imbibition times (Fig. 10) demonstrates that oil saturation declines slowly during the first 12 h, followed by a sharp decrease before eventually stabilizing with prolonged imbibition.

In addition, the wettability alteration during the imbibition process can be assessed based on the T_2 relaxation mechanism: the short T_2 peak (0.1–10 ms) corresponds to the adsorbed phase on the pore walls (bound water in a water-wet state, bound oil in an oil-wet state), while the long T_2 peak (10–1000 ms) corresponds to the free phase in the pore center (free oil in a water-wet state, free water in an oil-wet state). The extent of wettability alteration can be quantified using the mean T_2 value, the shift magnitude of the peak positions, and the peak area ratio. The initial mean T_2 value is 18.2 ms, corresponding to an oil-wet state: the short T_2 peak (0.9 ms) exhibits a weak signal, indicating that bound oil dominates the pore walls; the long T_2 peak is located at 26 ms, where the oil phase is in a semi-bound state and surface relaxation predominates. The variation trends of the long and short peaks during the imbibition process are shown in Fig. 11 and Table 5. During the displacement process, the mean T_2 value shows a slowly increasing trend

without an obvious inflection point: it rises to 19.1 ms at 3 days (an increase of 4.9%), to 20.0 ms at 9 days (an increase of 9.9%), and reaches 20.5 ms at 11 days, with a cumulative increase of 12.6%. The short T_2 peak shifts from 0.9 ms to 1.23 ms, indicating the gradual adsorption of the water phase to form bound water; the long T_2 peak shifts from 26 ms to 32 ms, suggesting that the oil phase is slowly transitioning toward the pore center. The test results are consistent with those from the rock slice tests [29–31].

Table 4: Core sample parameters.

Length (cm)	Diameter (cm)	Porosity (%)	Permeability (mD)
4.94	2.530	1.354	0.226

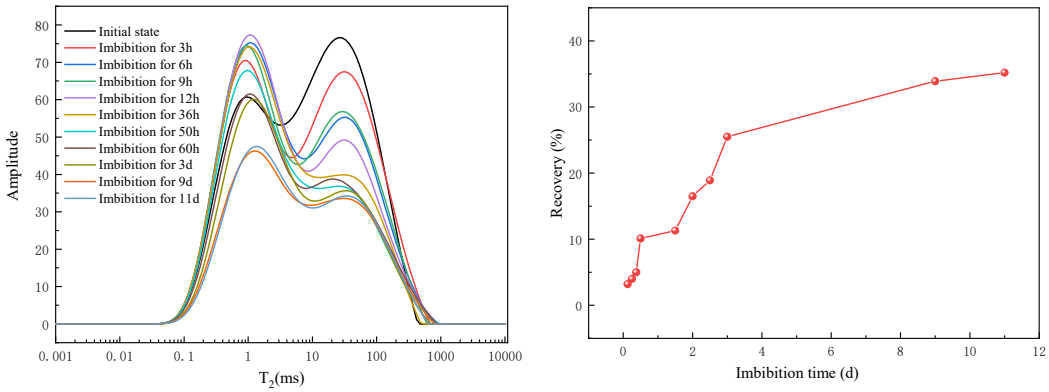


Figure 9: Changes in T_2 spectrum during the imbibition process and the corresponding oil recovery.

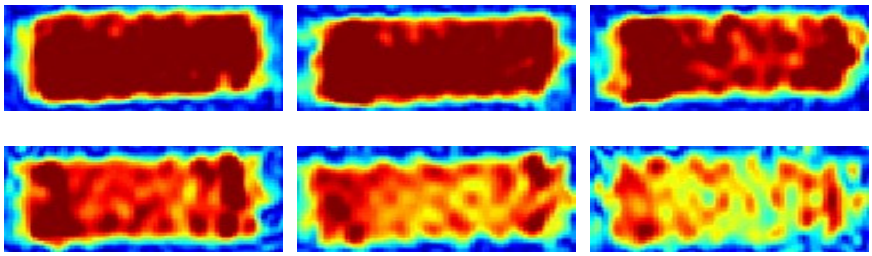


Figure 10: Two-dimensional imaging at different imbibition times (0 d, 6 h, 12 h, 36 h, 9 d, 11 d).

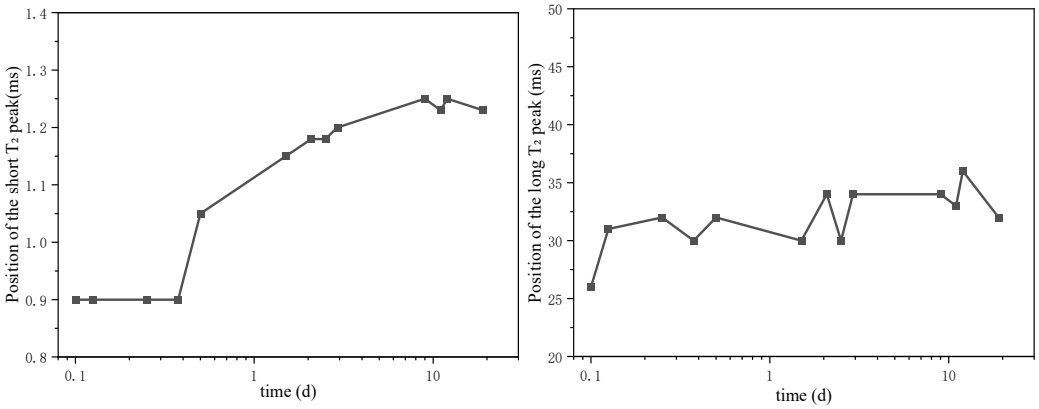


Figure 11: Variation trend of short/long T_2 peak positions.

Table 5: Key indicators during the imbibition and displacement process.

Indicators	Initial State (0 d)	Final State (11 d)	Shift Magnitude
Mean T_2 value (ms)	18.2	20.5	+12.6%
Position of the short T_2 peak (ms)	0.9	1.23	+36.7%
Position of the long T_2 peak (ms)	26	32	+23.1%

4 Conclusion

(1) Active silicon quantum dots can synergistically enhance the performance with the on-site slickwater. Compared with the on-site slickwater alone, the constructed multifunctional pressure-driven displacement system (SQDMFF) exhibits a denser three-dimensional network structure, as well as higher system viscosity and viscoelasticity, which contributes to improved proppant-carrying capacity.

(2) As the sand ratio increases from 20% to 50%, the proppant concentration inside the fracture increases, and the interaction among proppant particles strengthens. The settling rate of quartz sand decreases from 3.1 cm/min to 0.5 cm/min, the height of the sand bank inside the fracture rises, and the horizontal displacement of the sand bank decreases.

(3) Active silicon quantum dots can significantly reduce the oil-water interfacial tension to the order of 10^{-2} mN/m, decrease the contact angle to 44.8°, effectively enhance the deformation and migration ability of crude oil during transport in porous media, and reduce its adhesion ability on the rock surface. Ultimately, the static imbibition oil recovery reaches 35.2%, indicating promising application potential.

It should be noted that the conclusions of this study are primarily based on laboratory-scale experiments; further field pilot tests are required to validate the applicability of the SQDMFF system under actual reservoir conditions.

Acknowledgement: Not Applicable.

Funding Statement: We are grateful to Oil & Gas Major Project of China (Grant No. 2025ZD1405300) and Open Fund (PLN202420) of State Key Laboratory of Oil and Gas Reservoir Geology and Exploitation (Southwest Petroleum University) for financial support for this work.

Author Contributions: Yuan Xu: conceptualization, methodology, writing—original draft. Rui Jiang: investigation, data curation. Shuowen Deng: visualization, formal analysis. Kun Ding: resources, validation. Zheng Yao: investigation, software. Yifeng Liao: methodology, supervision. Youquan Liu: project administration, funding acquisition. Qi Xu: writing—review & editing, supervision. Daijun Du: conceptualization, supervision, writing—review & editing. All authors reviewed and approved the final version of the manuscript.

Availability of Data and Materials: The data supporting this study are available from the corresponding author upon reasonable request.

Ethics Approval: Not applicable.

Conflicts of Interest: Given his role as Guest Editor of this journal, Daijun Du had no involvement in the peer review of this article and had no access to information regarding its peer review. Full responsibility for the editorial process for this article was delegated to another journal editor. The authors declare no other conflicts of interest.

References

1. Sun L, Zou C, Jia A, Wei Y, Zhu R, Wu S, et al. Development characteristics and orientation of tight oil and gas in China. Petrol Explor Dev. 2019;46(6):1073–87. [CrossRef].

2. Peng H, Yang J, Peng J, Han H, Gou X, Jia Y, et al. Influence of supercritical CO_2 on the physical property of tight sandstone. Petroleum. 2024;10(3):520–6. [CrossRef].
3. Li N, Zhu S, Li Y, Zhao J, Long B, Chen F, et al. Fracturing-flooding technology for low permeability reservoirs: a review. Petroleum. 2024;10(2):202–15. [CrossRef].
4. Du DJ, Zou BY, Pu WF, Wei X, Liu R. Injectivity and plugging characteristics of CO_2-responsive gel particles for enhanced oil recovery in fractured ultra-low permeability reservoirs. J Petrol Sci Eng. 2022;214:110591. [CrossRef].
5. He Y, Shang Y, Wu W, Wang X. Investigating recovery potential through depletion development of tight oil reservoirs via NMR technology. Energy Fuels. 2024;38(1):333–40. [CrossRef].
6. Xiao L, Hou J, Wang W, Raj I. Development of a novel high-temperature microemulsion for enhanced oil recovery in tight oil reservoirs. Materials. 2023;16(19):6613. [CrossRef].
7. Xia Z, Wang X, Xu R, Ren W. Tight oil reservoir production characteristics developed by CO_2 huff 'n' puff under well pattern conditions. J Petrol Explor Prod Technol. 2022;12(2):473–84. [CrossRef].
8. Zhu W, He X, Li Y, Lei G, Santoso R, Wang M. Impacts of fracture properties on the formation and development of stimulated reservoir volume: a global sensitivity analysis. J Petrol Sci Eng. 2022;217:110852. [CrossRef].
9. Helmy AG, Salem SK, Elnoby M. Sensitivity analysis of hydraulic fracturing parameters for optimum horizontal well spacing in tight oil reservoirs. Arab J Sci Eng. 2025;50(7):4813–32. [CrossRef].
10. Cai M, Wang W, Wang X, Zhao L, Zhang H. Characteristics of hydraulic fracture penetration behavior in tight oil with multi-layer reservoirs. Energy Rep. 2023;10:2090–102. [CrossRef].
11. Sun L, Fang M, Fan W, Li H, Li L. Transient pressure performance analysis of hydraulically fractured horizontal well in tight oil reservoir. Energies. 2024;17(11):2556. [CrossRef].
12. Xu J, Liu R, Liu H. Optimization of shut-in time based on saturation rebalancing in volume-fractured tight oil reservoirs. Petrol Explor Dev. 2023;50(6):1445–54. [CrossRef].
13. Wang Z, Zhao X, Yang Z, Xiao Q, Lan J. Modeling for volume-fracturing vertical wells in tight oil reservoir considering NMR-based research on imbibition. Lithosphere. 2022;2022:2730294. [CrossRef].
14. Han B, Cui G, Wang Y, Zhang J, Zhai Z, Shi Y, et al. Effect of fracture network on water injection huff-puff for volume stimulation horizontal wells in tight oil reservoir: field test and numerical simulation study. J Petrol Sci Eng. 2021;207:109106. [CrossRef].
15. Fan P, Liu Y, Lin Z, Guo H, Li P. Experimental study on the efficiency of fracturing integrated with flooding by slickwater in tight sandstone reservoirs. Processes. 2024;12(11):2529. [CrossRef].
16. Cai M, Wang W, Wang X, Kong C, Zhang M, Wang L. Inversion method for effective drainage volume of tight oil horizontal wells with volume fracturing based on production analysis. J Petrol Explor Prod Technol. 2026;16(1):13. [CrossRef].
17. Wang J, Zhou F, Bai H, Li Y, Yang H. A Comprehensive method to evaluate the viscous slickwater as fracturing fluids for hydraulic fracturing applications. J Petrol Sci Eng. 2020;193:107359. [CrossRef].
18. Chen W, He R, Li L, Bai J, Li Z, Wang T, et al. Spontaneous imbibition and oil displacement experimental investigation in fracture-matrix cores of tight sandstone reservoirs. Sci Rep. 2026;16(1):14070. [CrossRef].
19. Dou X, Xing G, Zhao X, Xiao Q, Liu X, Shi Y. The water flooding seepage mechanism in the inter-fractures of horizontal wells in tight oil reservoirs. Fluid Dyn Mater Process. 2025;21(2):427–44. [CrossRef].
20. Luo Z, Xia D, He T, Yu J, Wang Y, Zhang H, et al. Experimental study on the mechanism of oil displacement by imbibition of fracturing fluids in tight sandstone reservoirs. Geosyst Eng. 2025:1–18. [CrossRef].
21. Zhu X, Gao H, Xie Y, Qi Y, Zhang N, Peng X, et al. Study on microscopic production characteristics of crude oil in tight reservoirs displaced by CO_2-assisted fracturing fluid. Petrol Sci Technol. 2025;43(25):3834–52. [CrossRef].
22. Li J, Gao X, Yang L, Gong J, Duan T, Song F, et al. Study on crude oil displacement efficiency by fracturing fluid in tight sandstone reservoir. PLoS One. 2025;20(11):e0335233. [CrossRef].
23. Wasan DT, Nikolov AD. Spreading of nanofluids on solids. Nature. 2003;423(6936):156–9. [CrossRef].
24. Hama SM, Ali JA, Manshad AK. Green-synthesized zinc quantum dots from parsley leaves for enhanced oil recovery: improving IFT, wettability, and oil recovery performance. Petrol Sci. 2026;23(6):3519–38. [CrossRef].

25. Wang Z, Jia H, Geng X, Liu Y, Shen Z, Xu R, et al. Synthesis of smart temperature responsive silicon quantum dots to stabilize Pickering emulsion for enhancing oil recovery. Colloids Surf A Physicochem Eng Aspects. 2026;740:140231. [CrossRef].
26. Gholamzadeh Y, Hemmati-Sarapardeh A, Sharifi M. Wettability alteration of carbonate calcite using nitrogen doped graphene quantum dots for enhanced oil recovery. J Mol Liq. 2026;455:129553. [CrossRef].
27. Standard SY/T 5336-2006. Practices for cores analysis. Beijing, China: National Development and Reform Commission of P.R. China; 2006.
28. Chekalov A, Ivanova A, Sokolov A, Sukhorukov G, Cheremisin A, Yuan C. Novel encapsulated surfactants for enhanced oil recovery in carbonate reservoir conditions: interfacial and wetting behavior. Adv Geo-Energy Res. 2025;18(3):272–86. [CrossRef].
29. Wang M, Sun P, Xiao D, Wang M, Gao Y, Lu S, et al. Wettability and its controlling factors of mixed shale oil reservoirs: a case study of Permian Lucaogou Formation in jimusar sag. Lithosphere. 2021;2021(Special 1):9190823. [CrossRef].
30. Ovsepian M, Salami Y, Karamov T, Du D, Dobysh I, Cheremisin A, et al. Multifunctional nanofluids for enhanced oil recovery by simultaneous *in situ* mobility control and displacement efficiency improvement. Adv Geo-Energy Res. 2023;19(3):231–41. [CrossRef].
31. Du D, Hou S, Pu W, Li Q, Zhang Y, Li B, et al. Investigation on enhanced oil recovery potential of active nano-SiO_2 in high-temperature and high-salinity reservoirs at core and pore scale. Fuel. 2026;404:136363. [CrossRef].